

A DUAL-BAND TERAHERTZ METAMATERIAL BASED ON A HYBRID ‘H’-SHAPED CELL

Wanyi Guo^{1, 2, *}, Lianxing He¹, Hao Sun¹, Hongwei Zhao³, Biao Li⁴, and Xiao-Wei Sun¹

¹Key Laboratory of Terahertz Solid-State Technology, Shanghai Institute of Microsystem and Information Technology, Shanghai 200050, China

²Graduate University of the Chinese Academy of Sciences, Beijing 100049, China

³Shanghai Institute of Applied Physics, Shanghai 201800, China

⁴National Laboratory of Antennas and Microwave Technology, Xidian University, Xi’an, Shaanxi 710071, China

Abstract—We present a dualband terahertz metamaterial based on a hybrid ‘H’-shaped cell of different sizes. The proposed ‘H’-shaped metamaterial (HSM) structure, fabricated on a quartz (SiO₂) substrate, exhibits two intense electrical resonances at ~ 0.95 THz and ~ 1.26 THz, respectively. Extracted effective permittivity show negative values in 0.95–1.01 THz and 1.26–1.42 THz bands. Measured results from the terahertz time-domain spectroscopy (THz-TDS) experiments show good agreement with the simulated results.

1. INTRODUCTION

Electromagnetic (EM) metamaterials are fascinating artificial composites with embedded sub-wavelength metallic structures [1, 2]. Since the first experimental realization of THz metamaterial reported by Yen et al. in 2004 [3], metamaterials with negative permittivity and/or permeability have spurred a significant research interest in THz regime due to their exotic EM properties that are not readily available from conventional materials [4, 5]. The THz metamaterials have enabled the development of new devices possible utilization in many novel applications in THz regime, where most natural materials behave too weak

Received 14 January 2013, Accepted 19 March 2013, Scheduled 19 March 2013

* Corresponding author: Wanyi Guo (gwynh@mail.sim.ac.cn).

EM response to be used. For example, a metamaterial solid-state terahertz phase modulator was presented by Chen et al. in 2009 [6]. A perfect metamaterial absorber based on a split-ring-cross resonator was designed by Cheng et al. in 2010 [7]. And Choi et al. present a terahertz metamaterial with unnaturally refractive index in 2011 [8]. However, the operation of many reported THz metamaterials often exhibits EM interaction to THz wave in a single and narrow frequency band, becoming a major hurdle to realize the possible multi-band THz functional devices such as modulators, switchers, filters, molecular sensors, absorbers and so on. Realizing multi-band operation of metamaterials, especially in the THz regime, has thus attracted a strong research interest. Recently, a few works about dualband and multi-band THz metamaterials have been reported [9–18]. A double band left-handed metamaterial composed of an extended version of the S-shaped resonators at microwave frequencies was presented by Chen et al. in 2004 [9]. In 2006, Gorkunov et al. suggest double-resonant (binary) metamaterials composed of two types of magnetic resonant elements [11]. Ekmekci et al. proposed the micro-split SRR type unit cell structures to be used for multi-band and tunable metamaterial design in 2009 [15]. Ma et al. reported a novel dual band THz metamaterial based on a single patterned layer in 2011 [17]. And a dualband metamaterial absorber based with resonant-magnetic structures was presented by Lee and Lee in 2012 [18].

In this letter, we present a simple design of dualband THz metamaterial based on a hybrid hollow ‘H’-shaped sub-wavelength structure. The proposed ‘H’-shaped metamaterial (HSM), embedded with periodic ‘H’-shaped metallic rings in the quartz substrate, performs two distinct electric resonances at ~ 0.95 THz and ~ 1.26 THz. Negative values of permittivity in 0.95–1.01 THz and 1.26–1.42 THz bands are achieved.

2. DESIGN AND ANALYSES

Figure 1(a) shows the structure of the proposed hollow ‘H’-shaped metamaterial (HSM), one may consider that the HSM is composed of two oppositely wound ‘C’-shaped arms aside and a capacitive gap in the center. The gap in the center behaves as a capacitor, and the ‘C’-shaped arms work as inductors. In comparison, the hybrid ‘C’-shaped metamaterial (CSM), obtained by subtracting the two connecting metal bars of HSM, are also presented (Figure 1(b)). To achieve EM resonance in THz regime, the periodicity of the metallic sub-wavelength structure is chosen to be $158 \mu\text{m}$ and $168 \mu\text{m}$ in two perpendicular directions. The total structure is constructed on a 20-

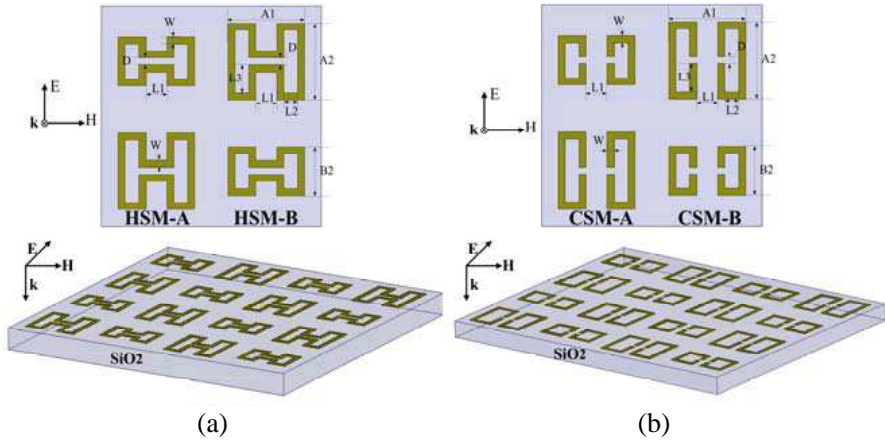


Figure 1. The designed structures of HSM and CSM. (a) HSM. (b) CSM.

μm -thick quartz (SiO_2) substrate, whose dielectric constant ϵ and loss tangent $\tan\delta$ are 3.78 and 0.001, respectively. And the metal array layer is gold with thickness of 300nm. The THz EM wave propagates at normal incidence (k in Figure 1) with the electric and magnetic fields completely parallel to the plane of metal layers. And the polarization of electric field is perpendicular to the gap between the two ‘C’-shaped arms. The finite element-based commercial electromagnetic field solver Ansoft HFSS is used for the simulation and optimization of the proposed structure. The optimized geometrical sizes of the proposed sub-wavelength structures in Figure 1 are: $W = 5 \mu\text{m}$, $D = 5 \mu\text{m}$, $L_1 = 15 \mu\text{m}$, $L_2 = 10 \mu\text{m}$, $L_3 = 20 \mu\text{m}$, $A_1 = 55 \mu\text{m}$, $A_2 = 55 \mu\text{m}$, $B_2 = 35 \mu\text{m}$.

The simulated magnitude and phase results of transmission (S_{21}) and reflection (S_{11}) coefficients of the proposed HSM are presented in Figures 2(a) and (b). In Figure 2(a), one can see two explicit transmission valleys near 0.95 THz and 1.26 THz. The minimums of S_{21} magnitude at the two transmission valleys are -18 dB and -23 dB , respectively. Correspondingly, two reflection peaks with phase mutation are also observed near 0.95 THz and 1.26 THz (Figure 2(b)). Based on the methods proposed by Smith [19], the effective relative permittivity and permeability can be obtained from the complex refractive index n and wave impedance z :

$$\epsilon = \frac{n}{z} = \epsilon' + i\epsilon'', \quad \mu = nz = \mu' + i\mu'' \quad (1)$$

$$n = \frac{1}{kd} \cos^{-1} \left[\frac{1}{2S_{21}} (1 - S_{11}^2 + S_{21}^2) \right] \quad (2)$$

$$z = \sqrt{\frac{(1 + S_{11})^2 - S_{21}^2}{(1 - S_{11})^2 - S_{21}^2}} \quad (3)$$

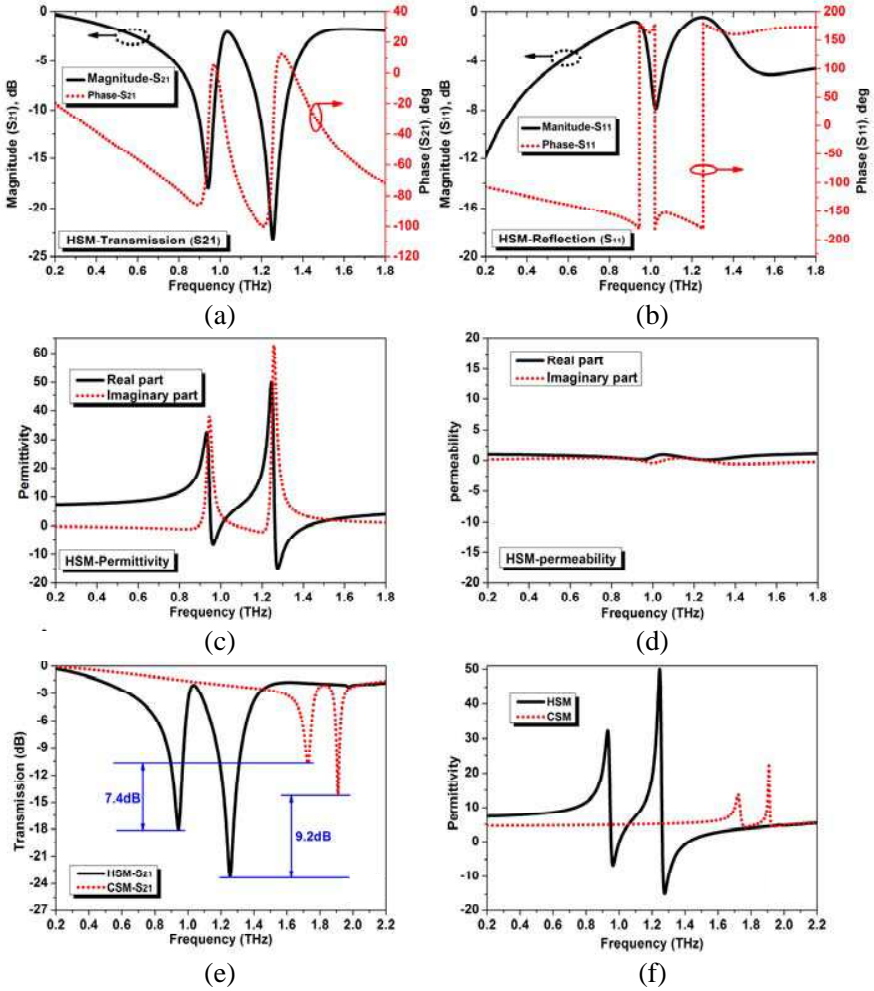


Figure 2. (a) Magnitude and phase of transmission (S_{21}) for HSM. (b) Magnitude and phase of reflection (S_{11}) for HSM. (c) Effective permittivity of HSM. (d) Effective permeability of HSM. (e) Magnitudes of transmission (S_{21}) of HSM and CSM. (f) Real parts of effective permittivity of HSM and CSM.

The S_{21} and S_{11} denote the transmission and reflection coefficients, respectively. $k = \omega/c$, ω is the radian frequency, d and c denote the slab thickness and the speed of light, respectively. In our paper, $e^{-j\omega t}$ is used as the time convention, and the positive imaginary permittivity/permeability implies loss. According to the formulas mentioned above, the effective permittivity and permeability are extracted and shown in Figures 2(c) and (d). The real part of effective permittivity performs negative value in two frequency bands of 0.95–1.01 THz and 1.26–1.42 THz, which are corresponding to the transmission valleys and reflection peaks with phase mutation in Figures 2(a) and (b). And the real part of permeability of the HSM performs positive value in the whole frequency band, which is shown in Figure 2(d). In comparison, the transmission and permittivity of CSM and HSM are shown in Figures 2(e) and (f). Due to its electrical resonance nature of the oppositely wound ‘C’-shaped split-rings, the transmission (S_{21}) in CSM reveals two sharp transmission valleys at ~ 1.72 THz and ~ 1.9 THz, respectively. One can see that the magnitude values of transmission (S_{21}) valleys in HSM are 7.4 dB and 9.2 dB lower than that in CSM at the two resonance frequencies respectively. It means that much stronger resonances are achieved by the connecting metal bars between two ‘C’-shaped arms. The two metal bars in the centre of HSM here supply an additional capacitor, which leads to the enhanced LC resonances with lower resonance frequencies of 0.95 THz and 1.26 THz.

To better understand the electric response of the experiment sample HSM to the EM wave of normal incidence, the surface current distribution of metallic plate at the resonance frequencies (~ 0.95 THz and ~ 1.26 THz) is shown in Figures 3(a) and (b). The black arrows and colourful ones demonstrate the different directions and densities of the surface current, respectively. Symmetrical circular current on the two ‘C’-shaped arms converges in and diverges from the two plates of the gap in the center, respectively. The induced surface current in two inductive ‘C’-shaped arms is oppositely wound and thus magnetic response is greatly weakened, which results in an almost net electric response. As a result, there is no significant mutation for the permeability. As can be seen in Figure 2(d), the real part of permeability is positive (the value around 1) and the imaginary part is almost around zero within the whole band. And the extremely weak magnetic resonance only makes the real and imaginary parts show some small deviations from the normal values (1 and 0 respectively). At the lower frequency resonance (~ 0.95 THz), the current density in the bigger unit cell (denoted as HSM-A) is much larger than that in the smaller unit cell (denoted as HSM-B). While at the

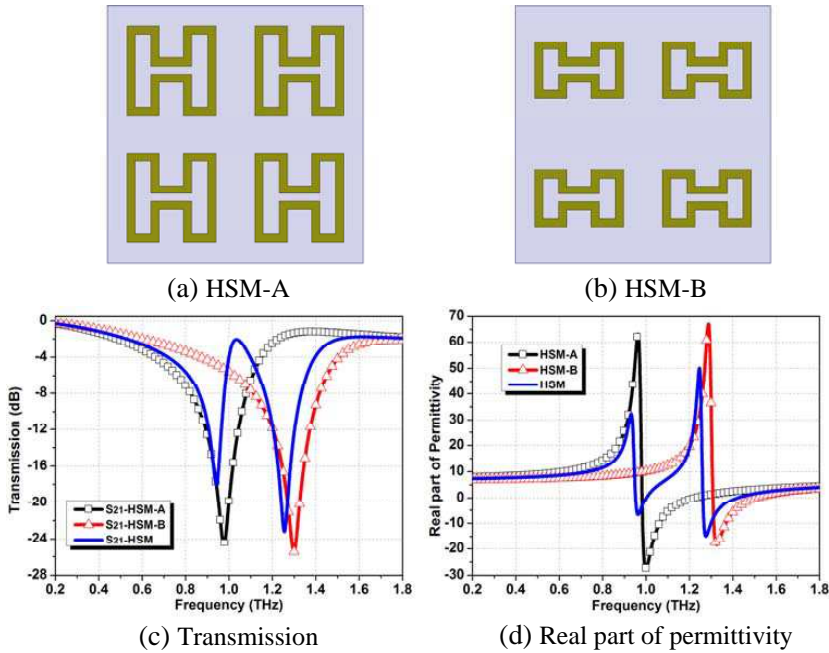


Figure 4. (a) Structure of HSM-A. (b) Structure of HSM-B. (c) Simulated transmission lines of HSM-A, HSM-B and HSM. (d) Real part of permittivity of HSM-A, HSM-B, and HSM.

reasonably agreed with the two resonances in HSM. So we can say that the two distinct resonances in HSM are really originated from HSM-A (the bigger cell) and HSM-B(the smaller cell), respectively.

To better understand the dual-band operation of the proposed hybrid ‘H’-shaped sub-wavelength structures, the HSM based on gallium arsenide (GaAs) substrate with the same thickness of $20\ \mu\text{m}$ is also analysed. Figure 5(a) shows the transmission lines of the GaAs and SiO_2 substrate without any metal layers. And Figure 5(b) shows the transmission (S_{21}) line and real part of permittivity of HSM based on GaAs substrate. One can see that the loss caused by the GaAs substrate (minimum of $-5.8\ \text{dB}$) is larger than that in SiO_2 substrate (minimum of $-1.9\ \text{dB}$). In addition, the transmission peak ($-5.1\ \text{dB}$) between the two transmission valleys of HSM-GaAs (in Figure 5(b)) is much lower than that of HSM- SiO_2 ($-1.8\ \text{dB}$ in Figure 2(a)). As shown in Figure 5(b), it is observed that two frequency bands with negative permittivity and transmission valleys also exist, which appear at lower frequencies of $0.56\ \text{THz}$ and $0.95\ \text{THz}$ due to the higher dielectric constants of GaAs than that of SiO_2 .

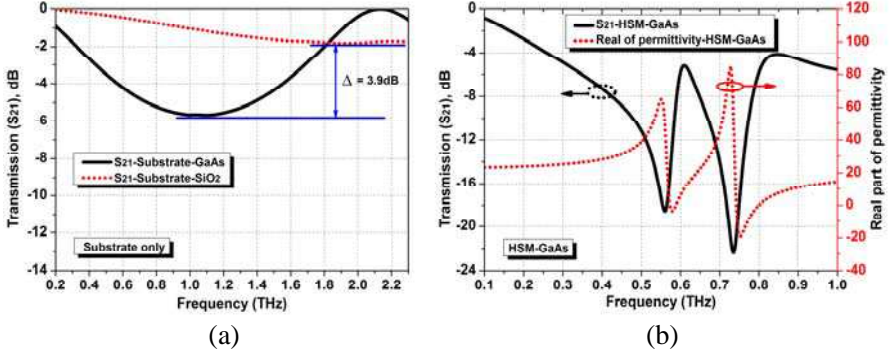


Figure 5. (a) Transmission of GaAs and SiO₂ substrates without metal layers. (b) Transmission and real part of permittivity of HSM-GaAs.

3. FABRICATION AND EXPERIMENT

The design and simulation results are verified by the fabrication and measurement of the proposed design. Figures 6(a) and (b) show the photographs of a portion of the fabricated samples of HSM-SiO₂ and HSM-GaAs under a microscope, and good fabrication quality is demonstrated. We fabricated the metal planar array pattern of HSM using photolithography and magnetron sputtering. To form the planar array pattern, S6809 of Shipley Co. and FHD320 of Fujifilm Co. were used as photoresist and developing solution, respectively. Before developing, we soaked the samples in chlorobenzene for 5 minutes to make them easier for liftoff. Then three metal layers, composed of Au/Pt/Ti with the thickness of 300/20/20 nm, were deposited on the 127- μ m-thick quartz (SiO₂) substrate and 350- μ m-thick gallium arsenide (GaAs) substrate by magnetron sputtering. The titanium layer was used to ensure a good adhesion to substrate, the platinum layer placed between titanium and gold was used to prevent the possible intermetallic diffusion. Liftoff technology was used to remove the unnecessary metals. The total size of each sample is 5 mm * 5 mm.

Measurements for the designed HSM samples are performed in Terahertz Time-Domain Spectroscopy (THz-TDS) at room temperature in a dry nitrogen atmosphere. The THz EM wave propagates at normal incidence (k in Figure 1) with the electric and magnetic fields completely parallel to the plane of metal layers. And the polarization of electric field is perpendicular to the gap between the two ‘C’-shaped arms. Fourier transform is used to calculate the frequency-domain results from the time-domain signal in the THz-

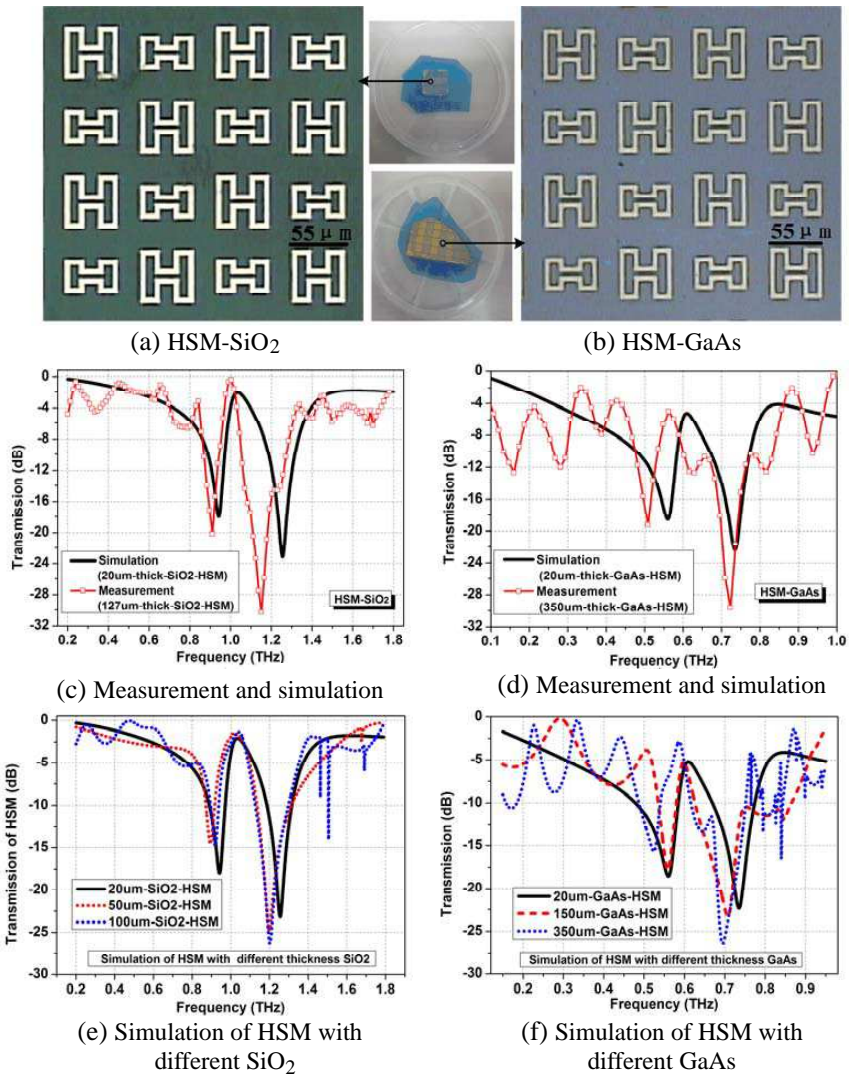


Figure 6. (a) The photograph of a portion of the fabricated HSM-SiO₂ under a microscope. (b) The photograph of a portion of the fabricated HSM-GaAs under a microscope. (c) Measured and simulated transmission of HSM-SiO₂. (d) Measured and simulated transmission of HSM-GaAs. (e) Simulated transmission of HSM with 20 μm-/50 μm-/100 μm-SiO₂. (f) Simulated transmission of HSM with 20 μm-/150 μm-/350 μm-GaAs.

TDS experiments. The measured and simulated transmissions for the designed HSM samples to THz wave are plotted in Figures 6(c) and (d). As for the two main transmission valleys, one can see that good agreements between the measured and simulated results for both of the HSM-SiO₂ and HSM-GaAs samples are achieved.

As shown in Figures 6(e) and (f), the simulated transmission spectra of HSM with different thicknesses substrates are similar except a few ripples. The ripples in the transmission spectra come from the Fabry-Perot resonances [20, 21], which are caused by the internal reflections within the two surfaces in the direction of propagation. And the thicker the substrate is, the lower the Fabry-Perot resonance frequency is. When studying the metamaterial performance caused by the periodic metal sub-wavelength structure, it is necessary to keep the Fabry-Perot resonance frequency far away from the designed frequencies. As a result, we designed and analyzed the HSM on 20- μm -thick quartz (SiO₂) and gallium arsenide (GaAs) substrates whose Fabry-Perot resonance frequencies are much higher than the as-designed frequencies. But it is difficult to fabricate the metal arrays on such a thin substrate of 20- μm -thickness and do the measurement with such thin samples. As a result, considering the fabrication conditions and difficulties in measurement, we fabricated the metal layers with hybrid ‘H’-shaped sub-wavelength structures on the 127- μm -thick quartz (SiO₂) substrate and 350- μm -thick GaAs substrate, and then do the measurement successfully. The measured results show good agreement with the simulated results.

4. CONCLUSIONS

In conclusion, we present the design, fabrication and experiment of a dual-band terahertz metamaterial based on a hybrid ‘H’-shaped cell with different sizes, and each cell is constructed by connecting two oppositely wound ‘C’-shaped arms aside and a capacitive gap in the center. The proposed ‘H’-shaped metamaterial (HSM) based on a quartz substrate exhibits two intense electrical resonances at ~ 0.95 THz and ~ 1.26 THz when the THz wave propagates normally to the metallic array surface and the THz electric field is perpendicular to the split gap (E). Measured results obtained from the THz-TDS experiments show good agreement with the simulated results. Based on the strong electric-field-coupling, negative values of permittivity in a two bands 0.95–1.01 THz and 1.26–1.42 THz are achieved. The proposed THz metamaterial could be a meaningful candidate for the potential multiband THz applications.

ACKNOWLEDGMENT

This work was supported by the National Basic Research Program of China (973) (Grant No. 2009CB320207).

REFERENCES

1. Veselago, V. G., "The electrodynamics of substances with simultaneously negative values of permittivity and permeability," *Sov. Phys. Usp.*, Vol. 10, No. 4, 509–514, 1968.
2. Pendry, J. B., A. J. Holden, D. J. Robbins, and W. J. Stewart, "Magnetism from conductors and enhanced nonlinear phenomena," *IEEE Trans. Microw. Theory Tech.*, Vol. 47, No. 11, 2075–2084, 1999.
3. Yen, T. J., W. J. Padilla, N. Fang, D. C. Vier, D. R. Smith, J. B. Pendry, D. N. Basov, and X. Zhang, "Terahertz magnetic response from artificial materials," *Science*, Vol. 303, No. 5663, 1494–1496, 2004.
4. Padilla, W. J., A. J. Taylor, C. Highstrete, M. Lee, and R. D. Averott, "Dynamical electric and magnetic metamaterial response at terahertz frequencies," *Phys. Rev. Lett.*, Vol. 96, 107401(1)–107401(4), 2006.
5. Tuniz, A., B. T. Kuhlmeiy, R. Lwin, A. Wang, J. Anthony, R. Leonhardt, and S. C. Fleming, "Drawn metamaterials with plasmonic response at terahertz frequencies," *App. Phys. Lett.*, Vol. 96, 191101(1)–191101(3), 2010.
6. Chen, H.-T., W. J. Padilla, M. J. Cich, A. K. Azad, R. D. Averitt, and A. J. Taylor, "A metamaterial solid-state terahertz phase modulator," *Nature Photonics*, Vol. 3, 148–151, 2009.
7. Cheng, Y., H. Yang, Z. Cheng, and N. Wu, "Perfect metamaterial absorber based on a split-ring-cross resonator," *J. Appl. Phys. A*, Vol. 102, 99–103, 2010.
8. Choi, M., S. H. Lee, Y. Kim, S. B. Kang, J. Shin, M. H. Kwak, K.-Y. Kang, Y. Hee, N. Park, and B. Min, "A terahertz metamaterial with unnaturally high refractive index," *Nature*, Vol. 470, No. 09776, 369–373, 2011.
9. Chen, H.-S., L.-X. Ran, J. Tao, F. Huang, X.-M. Zhang, and K.-S. Chen, "Metamaterial exhibiting left-handed properties over multiple frequency bands," *J. Appl. Phys.*, Vol. 96, 5338, 2004.
10. Sydoruk, O., O. Zhuromskyy, E. Shamonina, and L. Solymar, "Phono-like dispersion curves of magnetoinductive waves," *App. Phys. Lett.*, Vol. 87, 072501, 2005.

11. Gorkunov, M. V., L. V. Shadrivov, and Y. S. Kivshar, "Enhanced parametric processes in binary metamaterials," *Appl. Phys. Lett.*, Vol. 88, 071912, 2009.
12. Wen, Q. Y., H. W. Zhang, Y. S. Xie, Q. H. Yang, and Y. L. Liu, "Dual band terahertz metamaterial absorber: Design, fabrication, and characterization," *App. Phys. Lett.*, Vol. 95, 241111(1)–241111(3), 2009.
13. Yu, Y., C. Bingham, T. Tyler, S. Palit, R. Hand, W. J. Padilla, N. M. Jokerst, and S. A. Cummer, "A dual-resonant terahertz metamaterial based on single-particle electric-field-coupled resonators," *App. Phys. Lett.*, Vol. 93, No. 19, 19110(1)–19110(3), 2008.
14. Yu, Y., C. Bingham, T. Tyler, S. Palit, T. H. Hand, W. J. Padilla, D. R. Smith, N. M. Jokerst, and S. A. Cummer, "Dual-band planar electric metamaterial in the terahertz regime," *Opt. Express*, Vol. 16, No. 13, 9746–9752, 2008.
15. Ekmekci, E., K. Topalli, T. Akin, and G. Turhan-Sayan, "A tunable multi-band metamaterial design using micro-split SRR structures," *Opt. Express*, Vol. 17, No. 18, 16406–16058, 2009.
16. Tao, H., C. M. Bingham, D. Pilon, K. Fan, A. C. Strikwerda, D. Shrekenhamer, W. J. Padilla, X. Zhang, and R. D. Averitt, "A dual band terahertz metamaterial absorber," *J. Appl. Phys.*, Vol. 43, 225102–225106, 2010.
17. Ma, Y., Q. Chen, J. Grant, S. C. Saha, A. Khalid, and D. R. S. Cumming, "A terahertz polarization insensitive dual band metamaterial absorber," *Opt. Lett.*, Vol. 36, No. 6, 945–947, 2011.
18. Lee, H.-M. and H.-S. Lee, "A dualband metamaterial absorber based with resonant-magnetic structures," *Progress In Electromagnetics Research Letters*, Vol. 33, 1–12, 2012.
19. Smith, D. R., D. C. Vier, T. Koschny, and C. M. Soukoulis, "Electromagnetic parameter retrieval from inhomogeneous metamaterials," *Phys. Rev. E*, Vol. 71, 036617(1)–036617(11), 2005.
20. Han, N. R., Z. C. Chen, C. S. Lim, B. Ng, and M. H. Hong, "Broadband multi-layer terahertz metamaterials fabrication and characterization on flexible substrates," *Opt. Express*, Vol. 19, No. 8, 6991–6998, 2011.
21. Guo, W., L. He, B. Li, T. Teng, and X.-W. Sun, "A wideband and dual-resonant terahertz metamaterial using a modified SRR structure," *Progress In Electromagnetics Research*, Vol. 134, 289–299, 2013.